DOI: https://doi.org/10.2138/am-2022-8441. http://www.minsocam.org/

Word Count: 5471

Revision 2

Witness to Strain: Subdomain Boundary Length and the Apparent Subdomain Boundary Density in Large Strained Olivine Grains

Yaozhu Li[1,2], Phil J. A. McCausland[1,2], Roberta L. Flemming[1,2], and Callum J. Hetherington[3]

[1]*Department of Earth Sciences, Western University, London, ON, N6A 3K7, Canada*

[2]*Institute for Earth and Space Exploration, Western University, London, ON, N6A 3K7, Canada*

[3]*Department of Geoscience, Texas Tech University, Lubbock, Texas, 79409, the United States*

Abstract

Electron Backscatter Diffraction (EBSD) investigation of strain mainly uses polycrystalline samples to study fabric development. We extend the use of EBSD for analysis of large single mineral grains, by measuring the apparent surficial subdomain boundary density per unit area, reported here as Unit Segment Length (USL). We apply this USL technique to examine and quantify the plastic deformation recorded by naturally shocked olivine in the low to moderately shocked ureilite meteorite Northwest Africa 2221 and the highly-shocked martian dunitic cumulate meteorite Northwest Africa 2737, by assessing the types of subdomain boundaries and the increase of subdomain misorientation with increasing shock metamorphism. We further compare USL results for the shocked olivine in the meteorites with those for terrestrial deformation of Hawaiian olivine. USL of olivine increases with shock level, and USL from shocked olivine is significantly greater than that of terrestrially deformed olivine. USL is a promising tool for the quantification of plastic deformation in large single crystals, from shock as well as terrestrial deformation. The results derived from USL measurements along with local EBSD maps are complementary with quantitative 2D X-ray diffraction analysis of crystal deformation and disruption, leading to a more comprehensive understanding of characteristic shock deformation recorded by large single crystals.

Keywords: EBSD, crystal deformation, subdomain walls, shock metamorphism

DOI: https://doi.org/10.2138/am-2022-8441. http://www.minsocam.org/

Introduction

Hyper-velocity impacts cause shock metamorphism and deformation in rock. Impact events release enormous kinetic energy nearly instantaneously, which can vaporize and melt rocks, as well produce heat and do mechanical work on rocks that remain in the solid phase (Melosh 1989, Fritz et al., 2017). For individual mineral grains in a target rock, the impact may be recorded as crystal damage and deformation during the pressure pulse, and in post-shock plastic deformation, producing highly strained crystals (French, 1998).

The effects of shock in single crystals are largely recognized microscopically by petrographic textures in minerals, such as undulatory extinction, mosaicism, or recrystallization (Stöffler et al. 1991, 2018; French 1998; Fritz et al. 2017). Optically, non-strained crystals show complete extinction at a single orientation (also called straight extinction) under cross polarized light (XPL). A mosaic spread of crystal subdomain orientations is observed optically in XPL as undulatory extinction (a wave of extinction sweeping through the grain) or mosaicism (patchy extinction) when observed in thin section. Single crystals may also exhibit the development of planar fractures, planar deformation features and patchy amorphization (Stöffler et al. 1991, 2018; French 1998; Fritz et al. 2017).

Subdomain misorientation produced by shock deformation has also been reported by X-ray diffraction. Strain of single crystals as a mosaic spread of subdomain orientations is observed by X-ray diffraction as streaking of diffraction spots in two dimensional XRD patterns. This phenomenon is collectively described as strain-related mosaicity (SRM), with increased diffraction streak length correlated with greater shock level (Hörz and Quaide, 1973; Flemming, 2007; Izawa et al., 2011; Jenkins et al., 2019; Rupert et al., 2020; Li et al., 2020, 2021a).

These techniques are sensitive to degree of shock metamorphism, even allowing its quantification, but do not distinguish between shock-related strain in crystals and strain from geological processes. It is necessary to make the observations at the mesoscale to study shock effects on subdomains and their boundaries in crystals to investigate possible differences between strain mechanisms and establish the linkage to the petrographic observations and XRD.

In a distorted crystal, the excess free energy induced during shock metamorphism mobilizes dislocations by glide motion and produces strain in crystal structures (Cordier 2002). For unstrained crystals, statistically-distributed dislocations are balanced and would not contribute to grain surface curvature. For strained crystals, non-uniformly distributed dislocations are displaced forming subdomain boundaries and further misorienting subdomains, as a manifestation of accumulation of strain energy. The displacement mechanism is believed to be controlled by the glide motion at lower homologous temperatures (e.g. $T < 0.4T$ of melting point), and at higher temperatures, diffusion and climb effects also become more important (Boioli et al., 2015). This geometry of strain accommodation is known as geometrically necessary dislocations (GNDs) (Ashby 1970; Wheeler et al. 2009). The dislocation motion occurs along certain slip directions. In olivine, the orthorhombic crystal structure has three distinctive crystallographic axes where a-axis [100] and c-axis [001] are the most common directions for the creep behavior (Boioli et al., 2015). Dislocations have a vector line unit (**u**), and can further be characterized into edge and screw dislocations by the angle relationship with the slip direction (**b**). An edge dislocation has the characteristic that its unit vector is perpendicular to slip direction, whereas a screw dislocation has its unit vector parallel to slip direction (Fig 1).

Electron backscatter diffraction (EBSD) provides boundary information in crystalline samples when the step size is small enough (Prior et al. 1999; Wheeler et al. 2003, 2009). However, much current EBSD work has focused on polycrystalline samples and EBSD is less commonly applied to interrogate larger single grains. For example, the J-index and M-index derived from orientation and misorientation distribution functions are useful for analyzing lattice preferred orientation (LPO) and the fabric strength (Skemer et al. 2005; Bunge 2013). However, the J- and M-indexes have limited value during single crystal analysis because they show strong LPO regardless the deformation type.

Wheeler et al. (2003) presented the idea of using boundary geometry to study the boundary misorientation and anisotropy. Their work introduces the concept of boundary density by studying highly strained quartzite. Wheeler et al. (2009) later introduced the “weighted Burgers vector” technique to mathematically solve the problem of using EBSD to study dislocation gradients on a 2D orientation map by transforming the permutation tensor, setting the third-dimension perpendicular to the 2D map so that the gradient of the third dimension disappears. Wieser et al. (2020) applied this technique to identify subdomain wall types and the slip system type in strained olivine single crystals from Hawaiian magmatic mushes.

Based on these established procedures, we extend the use of 2D EBSD orientation mapping to investigate the apparent subdomain boundary density in highly strained olivine crystals. In practice, we directly measure the subdomain wall length from the EBSD orientation map and sum the measurable boundaries regardless of their type. The sum measurement is normalized to the measuring area so that it enables further comparison between different datasets. This measurement, called “Unit Segment Length (USL)”, is the examination of the apparent density of the subdomain walls in a single crystal contributed by geometrically necessary dislocations (GNDs). The inverted USL reflects subdomain sizes, and the similar approach was introduced to investigate the boundary anisotropy using boundary length by Wheeler et al. (2003). In this work, we calculate USL to directly represent the population of the subdomain boundaries within the surface area of the strained crystal, where a larger USL measurement indicates the presence of more subdomain boundaries and/or of greater subdomain boundary lengths. USL, therefore, is a useful quantitative assessment of the plastic deformation produced in high stress deformation regime, possibly by the glide motion of dislocations.

Sample Selection

To investigate the effectiveness of applying USL in a shock deformation study, we test USL on shocked coarse-grained olivine in meteorites Northwest Africa 2221 and Northwest Africa 2737. NWA 2221 is a low to moderately shocked ureilite (S3-S4), which is a primitive achondrite that consists of large olivine grains showing undulatory extinction (Irving 2005; Li et al. 2021). NWA 2737 is a martian chassignite, which is a dunitic cumulate rock. It consists of large olivine grains and is moderately to highly shocked (S5-S6), possibly during its ejection from Mars (Beck et al. 2006; Bläß et al. 2010; Li et al. 2021). Shock deformation features, e.g., undulatory extinction and mosaicism, in both meteorites in this work have been previously studied by quantitative XRD analysis and petrographic observations (e.g., Li et al. 2021). Shock pressure for the selected meteorites is greater than 25 GPa, therefore it is likely that subdomain boundaries observed by EBSD are largely developed through shock deformation with subdomain misorientation instead of other, crystal growth-related mechanisms such as dendritic growth texture.

To compare the effects of shock-induced deformation with terrestrial plastic deformation on subdomain misorientation, we also test USL on Hawaiian Kīlauea olivine reported by Wieser et al. (2020). Selection of the Hawaiian Kīlauea olivine has advantages over other terrestrial samples. First, they are olivine phenocrysts in a magma mush pile carried out by eruptive volcanic activities (Wieser et al., 2020), and the Hawaiian Kīlauea olivine EBSD data used in this study has been investigated by Wieser et al., (2020), in terms of deformation features, differential stresses, and extraction depth. Their work has shown that the observed microstructures in the mush pile olivine are formed by the differential stresses within volcanic plumbing systems under pressures of 3-12 MPa, and these textures are distinctive from dendritic growth as they lack phosphorous compositional zoning that is usually observed on olivine lattice distortion caused by compositional variation (Wieser et al., 2020). Importantly, Wieser et al. (2020) provide representative Hawaiian Kīlauea olivine EBSD data that are publicly available, allowing for comparison between the terrestrially deformed olivine in Weiser et al. (2020) and the shock-deformed olivine in this study in order to test the application of USL to characterize shock induced deformation in olivine.

Furthermore, for the shocked samples, we compare our USL results with X-ray based quantitative SRM analysis (e.g., Li et al., 2020) to test the consistency of observations between the two techniques.

Methods

Election Backscatter Diffraction

Electron backscatter diffraction (EBSD) data for NWA 2737 were acquired at McMaster University, Canadian Centre for Electron Microscopy. Data were collected using a JEOL JSM-7000F with a Schottky field emission gun and integrated Oxford Instruments X-Max 50 mm^2 EDS detector and Nordlys II EBSD Camera, providing resolution as fine as 1.2 nm at 30 keV and 3.0 nm at 1 keV. Data processing was performed using Aztec EDS/EBSD software plus HKL Channel EBSD software for the simultaneous acquisition of elemental and crystal orientation information. EBSD data acquisition for NWA 2221 was performed at Texas Tech University, College of Arts & Sciences Microscopy. Data were collected using a Zeiss Crossbeam 540 FEG-SEM, with an Oxford Instruments silicon drift detector (SDD) Energy Dispersive Spectrometer (EDS) and EBSD camera complemented by AZTec software that integrates packages by HKL. In this study, given the large olivine grains as targets, we collected electron diffraction data at a spacing of 2-3 μm depending on the size of grains to optimize collecting time and data resolution. To compare with terrestrial olivine, we apply the USL method on olivine data from Hawaiian magmatic mushes described by Wieser et al. (2020), and their EBSD data is available online along with their paper (Wieser et al., 2020).

Unit Segment Length USL Calculation

All EBSD data were processed using MTEX, an open-source Matlab-based EBSD data processing toolbox providing efficient data processing. Before the USL calculation, grain and subdomain boundaries are calculated. Misorientation angles of adjacent grains (or subgrains) are associated with increasing strain that reaches the "steady-state" at high misorientation angles in olivine (Poirier and Nicolas, 1975). Conventionally, high misorientation angle (>10-15°) boundary contacts are usually used to recognize a grain boundary and small misorientation angle (<15°) contacts are considered as subdomain boundaries (Poirier and Nicolas, 1975; Wieser et al., 2020). In this work, grain boundaries are set by a misorientation angle greater than 15°, and the inner, subdomain boundaries are recognized within the range of [0.5°, 15°] misorientation angle.

This is the peer-reviewed, final accepted version for American Mineralogist, published by the Mineralogical Society of America.
The published version is subject to change. Cite as Authors (Year) Title. American Mineralogist, in press.
DOI: https://doi.org/10.2138/am-2022-8441. http://www.minsocam.org/

Before reconstructing the inner boundary distribution, a denoising process is completed by applying the "halfQuadratic" filter to minimize the random errors caused by the deviation from the true orientation induced by a noisy Kikuchi pattern match or algorithm indexing. The necessity of this step, even when the data are not sparse, is discussed by several past works on EBSD data handling with the MTex toolbox (e.g., Hielscher et al. 2019a, 2019b)). The halfQuardratic filter uses the definition of total variation denoising that is based on principal signals to remove excessive noise while preserving the detail (Hielscher et al. 2019a). In this work, the filter is ideal to denoise the EBSD data for subdomain orientation investigation as it is designed to preserve the sub-boundary information.

We further apply the grain size filter to select subdomains with size greater than 2 pixels. Subdomain boundary segments are selected with misorientation angles greater than 0.5° and the minimum dislocation length greater than 1 micrometer. Since the 2-dimensional EBSD map only provides the trace of the grain boundaries, we consider steep dip boundaries only, given that the shallow boundaries are not likely to be observed. Herein, we only consider boundaries for which the misorientation axis is dipping greater than 15˚ relative to the sample surface.

To quantitatively indicate the apparent boundary density on 2D orientation maps, Unit Segment Length (USL) is calculated by summing all the selected boundaries and normalizing by the size of the total measured area. The unit of USL is inverse micrometer (μm^{-1}) as it is calculated by the total length of subdomain walls (μm) over the measured area (μm^{2}). The USL measurement reflects the subdomain boundary lengths contained within the unit measured area, enabling comparison between different samples.

Subdomain boundary type determination

Geometrically necessary dislocations (GNDs) form subdomain walls, and usually subdomain walls are considered as a "tilt wall" or "twist wall" depending on the dislocation types (edge or screw, respectively). In practice it is possible to have mixtures of both dislocations (Cordier 2002; Wheeler et al. 2009; Wieser et al. 2020).

Two-dimensional EBSD orientation maps only provide the trace of the subdomain boundaries on the investigated polished surface, therefore, without the information of the full geometry of subdomain walls, it is difficult to determine the exact subdomain boundary types. Nevertheless, it is possible to infer the boundary type based on the characteristics of two types of dislocation. Pure twist boundaries formed exclusively by screw dislocations have the rotation axis perpendicular to grain boundary walls, hence geometrically, the rotation axis must also be normal to the trace of grain boundaries and this perpendicular relationship may be identified on 2D EBSD maps. Hence, the boundary type may be estimated by mapping out the change of the intersection angle between misorientation axis and boundary trace direction (Fig. 1). The intersection angles approaching 90° indicate a twist boundary and the rest are mixtures and/or tilt boundaries. A similar approach was used by Wieser et al., (2020) to determine the amount of two types of boundaries by setting the limit of the intersection angle. Nevertheless, some boundaries were ignored by their approach. In this work, we color-code the angle change of the misorientation axis with respect to boundary trace, indicating the mixture of the two types of boundaries. There is a large mixture of twist wall and tilt wall in shocked meteorites, therefore we recommend using all the boundaries regardless their type, to calculate USL, thus reflecting the bulk degree of deformation.

Results

Boundary property and the apparent subdomain boundary density

As argued above, the exact type of subdomain wall is impossible to determine on the 2D EBSD map, but it is possible to infer type based on the angle of misorientation axis in sample rotation coordinates and the boundary trace direction. As shown in Fig. 2A, 2B, and 2C, subdomain boundaries are plotted with change of color according to the different intersection angles between the misorientation axis and boundary traces. A twist wall has a characteristic geometry such that its misorientation axis in sample rotation is normal to boundary trace, so only the boundaries in bright yellow color in Fig 2A, 2B and 2C are "pure" twist walls. As shown in Figure 2, the majority of boundaries are a mixture of both types of dislocation, but tilt boundaries are dominant, because the calculated misorientation axis-to-boundary trace angles are small.

Moreover, the boundary segment length also displays a large difference in shocked and unshocked sample. We observe a sharp decrease of the segment length from 10 μm to 1.5 μm in terrestrial Hawaiian olivine and NWA 2737, respectively (Fig 2A to 2C). It is evident in our shocked samples that subdomain boundaries are dominated by much shorter segments. Herein, we set the minimum boundary segment length threshold for all samples to 1 μm to include most of the boundaries in the USL calculation.

To avoid ambiguity of determining wall types and to enable full investigation of all subdomain boundaries, we adopt a robust way to calculate the USL by considering all subdomain walls (all boundaries in Figure 2A, 2B and 2C), regardless of their classification, and this all-inclusive calculation is called USL_{robust}. As such, USL_{robust} is the direct indicator of the subdomain boundary population that is created by shear forces during shock and plastic deformation. Larger USL_{robust} implies a larger population of subdomains in the distorted olivine crystals.

A significant difference is observed between USL_{robust} for shocked meteorites and non-shocked terrestrial olivine. Between shocked meteorites, the more highly shocked sample provides a larger USL. Specifically, three large olivine grains examined on ureilite NWA 2221 were tested and USL_{robust} measurements on the selected grains are 1.62×10^{-2} μm^{-1}, 3.40×10^{-2} μm^{-1} and 3.40×10^{-2} μm^{-1} respectively yielding the mean USL_{robust} of $2.81 \pm 1.03 \times 10^{-2}$ μm^{-1} (Table 1). Four large olivine grains on martian chassignite NWA 2737 were tested, and USL measurements are 5.38×10^{-2} μm^{-1}, 4.13×10^{-2} μm^{-1}, 5.26×10^{-2} μm^{-1}, and 6.74×10^{-2} μm^{-1}respectively, yielding a mean USL_{robust} of $5.38 \pm 1.07 \times 10^{-2}$ μm^{-1}(Table 1). Terrestrial olivine from Wieser et al. (2020) yields a USL_{robust} of 0.35×10^{-2} μm^{-1}, which is significantly smaller than those of the shocked samples (Table 1).

Estimation of boundary types and effects on USL

As demonstrated above, the ambiguity of determining boundary types cannot be easily resolved on a 2D map due to inadequate boundary trace information with depth. In this work, we use all subdomain walls when using USL to study the subdomain wall density in distorted crystals. Nevertheless, it is possible to estimate the amount of each type of wall by setting up angle leniency and calculating the USL accordingly. Here we present the estimation of walls primarily using the same angle leniency criteria as Wieser et al. (2020), where the setup ignores shallow dipping angle boundaries (<15°) and allows 15° angle leniency limits (to normal, or 75° as the minimum angle of misorientation axis and boundary trace) when determining the twist wall. Tilt wall is inferred by boundaries that are not twist wall with steep angle (>15°). More detail may be found in Wieser et al., (2020).

Not all boundaries are identified as either tilt or twist wall (as in Figure 1D, 1E, and 1F, where a red solid line represents tilt wall and a green solid line presents twist wall). Specifically,

This is the peer-reviewed, final accepted version for American Mineralogist, published by the Mineralogical Society of America.
The published version is subject to change. Cite as Authors (Year) Title. American Mineralogist, in press.
DOI: https://doi.org/10.2138/am-2022-8441. http://www.minsocam.org/

for NWA 2221, 91.2% of boundaries are identified, and among which, an average of 75% of the identified walls are tilt wall; for NWA 2737, 86% boundaries are identified and the tilt wall among identified boundaries has an average of 67%. For comparison, terrestrial olivine used in Wieser et al. (2020) 86% boundaries are identified, and the tilt wall percentage is 81% (Table 1). Tilt wall is the dominant subdomain wall type for all samples, but is notably more prevalent for Kīlauean olivine than for the two shocked meteorites. It is also notable that the proportion of tilt wall boundaries (estimated with angle limits suggested by Wieser et al., 2020) decreases with increasing shock level, suggesting that increasing shock level results in increasingly complex forms of crystal deformation.

To further investigate the observation, we separate the boundary trace according to the Burgers vectors [100] and [001] as they are the dominant active slip directions for olivine. We observe that the shocked sample subdomain boundaries show the twist property formed by screw dislocation (Fig 2E and 2F) ubiquitously in both directions. In contrast, Hawaiian olivine shows dominant edge characteristics overall.

The difference between USL_{robust} and $USL_{(Tilt + Twist)}$ is small and the overall trend for different shocked samples is also similar. NWA 2221 yields an average $USL_{(Tilt + Twist)}$ of $2.58 \pm 0.99 * 10^{-2}\ \mu m^{-1}$, NWA 2737 yields an average $USL_{(Tilt + Twist)}$ of $4.64 \pm 0.92 * 10^{-2}\ \mu m^{-1}$, and terrestrial olivine has an average $USL_{(Tilt + Twist)}$ of $0.31*10^{-2}\ \mu m^{-1}$. All measurements are summarized in Table 1.

Discussion

Interpretation of Unit Segment Length Measurements and Shock Deformation

Previous EBSD work has largely focused on the identification of lattice preferred orientation and fabric strength in polycrystalline samples, and its application is limited when applied to single crystal analysis because single grains are likely to give strong preferred orientation regardless the deformation regime. The slip system identification framework in single crystals developed by Wheeler et al. (2009) and Wieser et al. (2020) provided successful attempts to apply EBSD to single crystal analysis, and our work further expands the application of EBSD to single crystals to study shock and local plastic deformation in a quantitative manner.

Unit Segment Length is a simple, direct, and quantitative method that allows the users to compare different shocked and deformed samples, in order to study the effect of shock waves and deformation type. Boundary traces are measured on a 2D EBSD map, and it is crucial to consider all boundary types for the full subdomain boundary density estimation during single crystal analysis. Unlike the boundary density work demonstrated by Wheeler et al., (2003), USL is not designed to reflect directional information, it is instead a quantitative measurement of the density of boundaries in all orientations.

The results determined by USL are an indicator of the apparent subdomain boundary density in the investigated grain, as far as can be determined by extension from the 2D surface. It is designed to quantify the length and density of domain boundaries, and the measurement considers all the subdomain boundaries regardless of their direction.

The deformation and microstructure development in olivine is usually characterized as steady state dislocation creep where stress becomes constant and is independent of plastic strain, when forming high angle boundary contacts (>10°-15°) (Poirier and Nicolas 1975; Thieme et al. 2018). Subdomains, however, are primarily considered as having low angle contacts (<15°) formed before reaching the steady state during the stage of “transient creep” (Thieme et al.

2018). In this work, large USL values indicate the accumulation of plastic strain, forming subdomain boundaries by deformation stresses.

Effects of shock metamorphism in the meteorites are produced by shock waves unloading transient overpressure in the solid (Fritz et al., 2017). Terrestrial rock usually experiences a slow strain rate over long deformation time, such as tectonism with strain rate around 10^{-15}/s (Korenaga and Karato 2008). Shocked rock experiences rapidly increased particle velocity, applied stress and local material density change with the passage of the shock front, in which the strain rate can be up to 10^{6}/s (Fritz et al., 2017). During the passage of the shock front, minerals within the rock take up deformation where the amplitudes of the shock wave exceed the elastic limits of the rock, resulting in permanent plastic deformation. Rapid volume compression and decompression increases the misorientation in the crystal structure leading to the destructive effects observed in shocked meteorites. Petrographically, these effects are observable as mineral textures in shocked meteorites such as fractures, increased dislocations, undulatory extinction, mosaicism, and planar deformation features (Stöffler et al. 1991, 2018; Fritz et al. 2017; Li et al. 2021a).

The high density of the accumulated subdomain walls observed in meteorites in this work suggests that shock-related strain is stored in a large range of small misoriented subdomains in shocked crystals. We consider the large USL measurement to represent the shock-induced disturbance of the strained crystal. These observations are consistent with shock classification of NWA 2221 (S3-S4) and NWA 2737 (S5-S6) by petrographic observations and quantitative SRM analysis. NWA 2221 shows undulatory extinction and weak mosaicism as the result of shock-induced misorientation in the olivine crystals (Li et al. 2021a). NWA 2737 has shock-darkened brown olivine caused by nano-scale Fe particles precipitated in the olivine crystals (Beck et al., 2006; Bläß et al., 2010; Li et al., 2021b), with the Fe derived from the olivine crystal during high-pressure deformation (Van de Moortèle et al. 2007; Fritz et al. 2017), consistent with increased misorientation and subdomain development in the host olivine.

The effect of shock disturbance on misorienting subdomains in single crystals may also be monitored by the property change of the boundary segments (Fig 3). Among the samples examined, we observed that a shortened segment length correlates with the increase of USL with increasing shock deformation (Fig 3A to 3C). Notably, we also observed that angle changes between the boundary direction and misorientation axis for intermediate angles (between 30 to 60) significantly increase with increasing shock level, indicating the mixture of two types of dislocation is increased by the shock process that with a higher proportion of twist boundaries with higher shock level (Fig 3D to 3F). We made a similar observation when adopting the method of Wieser et al. (2020) to calculate the tilt ratio; the ratio dropped significantly between the non-shocked terrestrial sample and the highly shocked Martian chassignite (Table 1).

It has been proposed that lattice planes that glide along [100] Burgers vectors show more edge characteristics (Fig 3D), and [100] dislocation gliding on (010) and (001) planes has been interpreted from observations of long straight edge segments (Darot and Gueguen 1981; Gueguen and Darot 1982; Boioli et al. 2015; Wieser et al. 2020). In high stress deformation regimes, it is observed that c-axis screw (glide along [001]) becomes more dominant (e.g., Gueguen and Darot 1982), because the stress dependence of the activation energy becomes more important leading to a “glide-controlled” motion (Gueguen and Darot 1982). Similarly, we see more screw segments, even in [100] in the shocked samples (Fig 3E, 3F). These observations demonstrate that the destructive effects of shock deformation on crystal structure are strongly pressure-controlled and provide high shear stress that enhances the glide motion of lattice planes along its Burgers vectors, [100] and [001], activating the slip systems that feature more screw dislocations (Fig 3D to 3F).

The observation of the creation of the numerous small segments is consistent with the creation of small mosaic blocks observed by XRD, and the increased mixture of two types of dislocation shows the necessity of using all the possible boundaries when calculating USL.

Comparison with XRD quantitative strain-related mosaicity

Quantitative XRD strain-related mosaicity (SRM) has been discussed and applied in various examples, such as enstatite in enstatite chondrites (Izawa et al., 2011;), olivine and pyroxene in ordinary chondrites (McCausland et al., 2010; Jenkins et al.,2019; Rupert et al., 2020), plagioclase in lunar samples (Pickersgill et al., 2015), and olivine in ureilites (Yaozhu Li et al. 2021). Non-strained crystals produce single diffraction spots on 2D XRD images, however when a crystal is non-uniformly strained or bent, dislocations stored in the crystal migrate and form subdomain boundaries, producing a mosaic spread of diffraction orientations showing streaks along the Debye ring direction (χ) on 2D XRD images. In the case where large subdomains are formed, the streaks may further develop into a row of spots along the Debye ring, referred to as “asterism” in the 2D XRD image. Well-developed asterism in the 2D XRD image is comparable with the petrographic observation of mosaic texture in thin section where large subdomains are visible.

Diffraction textures are determined by the mosaic block sizes of the subdomains and the degree of subdomain misorientation. Discrete spot patterns are from very large undistorted crystals (>50 μm) indicating a single crystal and no misorientation (Fig 4). Homogenous streak patterns are thought to form from curved crystals with a myriad of slightly rotated very small

This is the peer-reviewed, final accepted version for American Mineralogist, published by the Mineralogical Society of America.
The published version is subject to change. Cite as Authors (Year) Title. American Mineralogist, in press.
DOI: https://doi.org/10.2138/am-2022-8441. http://www.minsocam.org/

mosaic blocks (< 5 μm) indicative of many very small slightly misoriented subdomains. Asterism patterns are rows of X-ray spots diffracted from relatively larger mosaic blocks (> 10 μm) implying the development of misoriented unstrained subdomains in the deformed crystals (Hörz and Quaide 1973; Flemming 2007; Vinet et al. 2011; Jenkins et al. 2019; Li et al. 2020; Li et al. 2021a). Quantitative strain related mosaicism analysis measures the Full Width Half Maximum or Sum of Full Width Half Maximum from peaks integrated from the patterns along the Debye rings or chi dimension (χ) as FWHMχ or Σ(FWHMχ), and more highly shocked crystals exhibit larger measurements (broader peaks have larger FWHMχ).

Quantitative SRM analysis on both meteorite samples used in this study have been reported previously (Li et al., 2021a,b). The sample with lower shock, ureilite NWA 2221, exhibited the streaky patterns on XRD images, and it yielded top 25% of all Σ(FWHMχ) measurements as 7.9°± 1.2° (N = 10) indicating the mild to moderate mosaic spread due to the subdomain misorientation (Li et al. 2021). The more highly shocked Martian chassignite NWA 2737 yielded top 25% of Σ(FWHMχ) of 15.7° ± 1.18° (N = 10) indicating an increase of subdomain misorientation (Li et al. 2021). Top 25% Σ(FWHMχ) measurements reflect the highest shock in the sample studied by XRD, consistent with the petrographic shock stage evaluation scheme of Stöffler et al. (1991, 2018). This observation is consistent with USL measurements in which NWA 2221 yields a USL_{robust} value of $2.81 \pm 1.03 * 10^{-2}\ \mu m^{-1}$compared with NWA 2737 which has a USL_{robust} of $5.38 \pm 1.07 * 10^{-2}\ \mu m^{-1}$, indicating an increase of the subdomain population with increasing shock level. The results from both methods suggest that more dislocations have migrated to form subdomain boundaries with an increasing degree of misorientation induced by a higher shock level.

DOI: https://doi.org/10.2138/am-2022-8441. http://www.minsocam.org/

USL measurement using EBSD complements XRD-based SRM techniques for measuring the degree of shock metamorphism in minerals. Specifically, quantitative SRM analysis provides information on the apparent mosaic block size and degree of misorientation for many minerals to represent the shock level in a rock whereas quantitative USL provides direct information on the apparent subdomain boundary density for each mineral grain investigated, opening a window for exploring shock deformation mechanisms. Together, both methods provide a quantitative measure and spatial representation of local deformation strain in distorted crystals.

Implications

This study provides an alternative way to examine strained crystals by extending the use of EBSD analysis to deformed single crystals. Unit segment length (USL) results from our collected data and previously published data show that USL is a powerful tool to estimate the subdomain wall population by reconstructing sub-boundary information from the EBSD 2D orientation maps.

We also demonstrate how the disruptive effects of shock change the property of the boundary trace by monitoring the segment length and its geometry, e.g., the angle between boundary trace and its misorientation axis. This observation is especially important for distinguishing shock deformation from terrestrial deformation. The presented data represent a small number of samples, but nevertheless suggest that shock deformation creates shortened segment length and produces more mixed boundaries of screw and edge dislocation (Fig 3).

Our results are consistent with petrographic observations and XRD-based SRM analysis, showing an increase of subdomain boundary density (as calculated by USL) with an increasing degree of shock deformation. Moreover, the significant difference observed between shocked olivine and terrestrially deformed olivine suggests that USL may be a useful tool to discriminate shock deformation (higher USL) from terrestrial deformation (lower USL), where both types of deformation tend to result in overlapping streak lengths in 2D XRD patterns, such that SRM analysis cannot distinguish shock metamorphism from terrestrial deformation (Vinet et al., 2011; Izawa et al., 2011). This finding helps to solve the uncertainty when distinguishing shock textures from terrestrial plastic deformation based on petrographic or micro-XRD observations.

Finally, the code developed in this work allows users to visualize the change of subdomain boundary type between tilt wall and twist wall. We monitor the angle change between boundary trace direction and misorientation axis in [100] and [001] direction. It enables the further assessment of the shock effects and provides a spatial and quantitative investigation of dislocation migration and subdomain boundary formation within a strained crystal.

Acknowledgements

We thank Dr. Chris Herd at University of Alberta for loaning us a sample of chassignite NWA 2737; we thank Chris Butcher at McMaster University for assisting with EBSD data collection on NWA 2737 and we thank Dr. Bo Zhao at Texas Tech University who assisted with EBSD data collection on NWA 2221. Reviews from Dr. John Wheeler and an anonymous reviewer were very helpful for focusing this contribution. PJAM and RLF thank the NSERC-Discovery Grant program for providing funding relating to this work. Y. Li thank the Science International Engagement Funding (Western University) and Mitacs Canada for providing funding related to this project.

(28866 characters, excluding abstract and spaces)

Data Availability

Codes developed in this work is available on the online repository Mendeley Data. A sample EBSD data and Matlab script file are provided. Full citation and the doi for the datasets are: Li, Yaozhu; McCausland, Phil J.A.; Flemming , Roberta L.; Hetherington, Callum J. (2022), “Unit Segment Length for olivine EBSD single grain analysis”, Mendeley Data, V1, doi: 10.17632/7kb9xhd4cz.2

REFERENCES

Ashby, M. (1970) The deformation of plastically non-homogeneous materials. The Philosophical Magazine: A Journal of Theoretical Experimental and Applied Physics, 21, 399–424.

Beck, P., Barrat, J.-A., Gillet, P., Wadhwa, M., Franchi, I., Greenwood, R., Bohn, M., Cotten, J., Van de Moortèle, B., and Reynard, B. (2006) Petrography and geochemistry of the chassignite Northwest Africa 2737 (NWA 2737). Geochimica et Cosmochimica Acta, 70, 2127–2139.

Bläß, U.W., Langenhorst, F., and McCammon, C. (2010) Microstructural investigations on strongly stained olivines of the chassignite NWA 2737 and implications for its shock history. Earth and Planetary Science Letters, 300, 255–263.

Boioli, F., Carrez, P., Cordier, P., Devincre, B., and Marquille, M. (2015) Modeling the creep properties of olivine by 2.5-dimensional dislocation dynamics simulations. Physical Review B, 92, 014115.

Bunge, H.-J. (2013) Texture analysis in materials science: mathematical methods. Elsevier.

Cordier, P. (2002) Dislocations and slip systems of mantle minerals. Reviews in Mineralogy and Geochemistry, 51, 137–179.

Darot, M., and Gueguen, Y. (1981) High-temperature creep of forsterite single crystals. Journal of Geophysical Research: Solid Earth, 86, 6219–6234.

Flemming, R.L. (2007) Micro X-ray diffraction (μXRD): a versatile technique for characterization of Earth and planetary materials. Canadian Journal of Earth Sciences, 44, 1333–1346.

French, B.M. (1998) Traces of catastrophe: A handbook of shock-metamorphic effects in terrestrial meteorite impact structures. Technical Report, LPI-Contrib-954.

Fritz, J., Greshake, A., and Fernandes, V.A. (2017) Revising the shock classification of meteorites. Meteoritics & Planetary Science, 52, 1216–1232.

Gueguen, Y., and Darot, M. (1982) Upper mantle plasticity from laboratory experiments. Physics of the Earth and Planetary Interiors, 29, 51–57.

Hielscher, R., Silbermann, C.B., Schmidl, E., and Ihlemann, J. (2019a) Denoising of crystal orientation maps. Journal of Applied Crystallography, 52, 984–996.

Hielscher, R., Bartel, F., and Britton, T.B. (2019b) Gazing at crystal balls: Electron backscatter diffraction pattern analysis and cross correlation on the sphere. Ultramicroscopy, 207, 112836.

Hörz, F., and Quaide, W.L. (1973) Debye-Scherrer investigations of experimentally shocked silicates. The Moon, 6, 45–82.

Irving, T. (2005) NWA 2221 Meteoritical Bulletin Classification. Antarctic Meteorite Newsletter, 21.

Izawa, M.R., Flemming, R.L., Banerjee, N.R., and McCAUSLAND, P.J. (2011) Micro-X-ray diffraction assessment of shock stage in enstatite chondrites. Meteoritics & Planetary Science, 46, 638–651.

Jenkins, L.E., Flemming, R.L., and McCausland, P.J. (2019) Quantitative in situ XRD measurement of shock metamorphism in Martian meteorites using lattice strain and strain-related mosaicity in olivine. Meteoritics & Planetary Science.

Korenaga, J., and Karato, S. (2008) A new analysis of experimental data on olivine rheology. Journal of Geophysical Research: Solid Earth, 113.

Li, Y., McCausland, P.J., and Flemming, R.L. (2020) Best Fit for Complex Peaks (BFCP) in Matlab® for quantitative analysis of in situ 2D X-Ray diffraction data and Raman spectra. Computers & Geosciences, 144, 104572.

Li, Y., McCausland, P.J.A., and Flemming, R.L. (2021a) Quantitative shock measurement of olivine in ureilite meteorites. Meteoritics & Planetary Science, 56, 1422–1439.

Li, Y, McCausland, P., and Flemming, R. (2021b) Shock Effects on Olivine Structure and Slip Systems in Martian Dunite Northwest Africa 2737 p. 2428. Presented at the Lunar and Planetary Science Conference.

McCausland, P., Flemming, R., and Izawa, M. (2010) Quantitative shock stage assessment in olivine and pyroxene bearing meteorites via in situ micro-XRD Vol. 1, p. 03. Presented at the AGU Fall Meeting Abstracts.

Pickersgill, A.E., Flemming, R.L., and Osinski, G.R. (2015) Toward quantification of strain-related mosaicity in shocked lunar and terrestrial plagioclase by in situ micro-X-ray diffraction. Meteoritics & Planetary Science, 50, 1851–1862.

Poirier, J., and Nicolas, A. (1975) Deformation-induced recrystallization due to progressive misorientation of subgrains, with special reference to mantle peridotites. The Journal of Geology, 83, 707–720.

Prior, D.J., Boyle, A.P., Brenker, F., Cheadle, M.C., Day, A., Lopez, G., Peruzzi, L., Potts, G., Reddy, S., and Spiess, R. (1999) The application of electron backscatter diffraction and orientation contrast imaging in the SEM to textural problems in rocks. American Mineralogist, 84, 1741–1759.

Skemer, P., Katayama, I., Jiang, Z., and Karato, S. (2005) The misorientation index: Development of a new method for calculating the strength of lattice-preferred orientation. Tectonophysics, 411, 157–167.

Stöffler, D., Keil, K., and Edward R.D, S. (1991) Shock metamorphism of ordinary chondrites. Geochimica et Cosmochimica Acta, 55, 3845–3867.

Stöffler, D., Hamann, C., and Metzler, K. (2018) Shock metamorphism of planetary silicate rocks and sediments: Proposal for an updated classification system. Meteoritics & Planetary Science, 53, 5–49.

Thieme, M., Demouchy, S., Mainprice, D., Barou, F., and Cordier, P. (2018) Stress evolution and associated microstructure during transient creep of olivine at 1000–1200 C. Physics of the Earth and Planetary Interiors, 278, 34–46.

Van de Moortèle, B., Reynard, B., McMillan, P.F., Wilson, M., Beck, P., Gillet, P., and Jahn, S. (2007) Shock-induced transformation of olivine to a new metastable (Mg, Fe) 2SiO4 polymorph in Martian meteorites. Earth and Planetary Science Letters, 261, 469–475.

Vinet, N., Flemming, R.L., and Higgins, M.D. (2011) Crystal structure, mosaicity, and strain analysis of Hawaiian olivines using in situ X-ray diffraction. American Mineralogist, 96, 486–497.

Wheeler, J., Jiang, Z., Prior, D., Tullis, J., Drury, M., and Trimby, P. (2003) From geometry to dynamics of microstructure: using boundary lengths to quantify boundary misorientations and anisotropy. Tectonophysics, 376, 19–35.

Wheeler, J., Mariani, E., Piazolo, S., Prior, D., Trimby, P., and Drury, M. (2009) The weighted Burgers vector: a new quantity for constraining dislocation densities and types using electron backscatter diffraction on 2D sections through crystalline materials. Journal of microscopy, 233, 482–494.

Wieser, P.E., Edmonds, M., Maclennan, J., and Wheeler, J. (2020) Microstructural constraints on magmatic mushes under Kīlauea Volcano, Hawaiʻi. Nature communications, 11, 1–14.

DOI: https://doi.org/10.2138/am-2022-8441. http://www.minsocam.org/

FIGURE CAPTIONS

Figure 1: Schematic illustration of boundary types. The figure is modified after Wieser et al., (2020). Fig 1A shows the tilt wall characteristic that its misorientation axis is parallel to the boundary trace. Fig 1B shows the twist wall characteristic that the misorientation axis is perpendicular to the boundary trace.

Figure 2: EBSD subdomain visualization and boundary types. Representative grains from NWA 2221 and NWA 2737 are selected to demonstrate subdomain misorientation and boundaries in shocked rocks. These are compared to terrestrial olivine EBSD data from Wieser et al., (2020). All grain areas are colored by an inverse pole figure coloring scheme to show subdomain orientation changes as shown in the inset. In Fig 2A, 2B, and 2C, all subdomain boundaries are colored to represent the angular difference between the boundary trace in the plane of section and the misorientation of sample rotation axis between subdomains. Perpendicular angular relationship is indicated by a bright yellow line color representing the endmember twist wall, whereas a dark blue line color represents endmember tilt wall, with the misorientation axis lying sub-parallel to the boundary trace. Most subdomain boundaries are a mixture of twist and tilt wall behavior. All boundaries are used to calculate USL_{robust}. A greater mixture of tilt and twist walls are observed in highly shocked NWA 2737, possibly representing a more complex shock deformation process. Fig 2D, 2E, and 2F show the boundary type estimation using angle leniency of 15° as described by Wieser et al. (2020). Lines in red color represent tilt wall and lines in green color represent twist wall.

This is the peer-reviewed, final accepted version for American Mineralogist, published by the Mineralogical Society of America.
The published version is subject to change. Cite as Authors (Year) Title. American Mineralogist, in press.
DOI: https://doi.org/10.2138/am-2022-8441. http://www.minsocam.org/

Figure 3: Histogram showing boundary property changes. A to C are histograms of boundary segment length corresponding to the sample in Figure 2. Y axis is the amount of measurements and X axis is the segment length in micrometers. D to F are histograms showing the boundary geometry change with respect to boundary direction and misorientation axis. Y axis is the amount of measurements and X axis is the angle between boundary trace and misorientation axis in degrees. Overall, shocked samples show much shortened boundary segments (3A to 3C). Fig 3D to 3E are color coded by a-axis slip (blue) and c-axis slip (orange). In both slip directions, angle between boundary trace and misorientation axis is increased indicating a potentially more twist wall-dominated properties in shocked samples.

Figure 4: Example 2D X-ray diffraction images for shock-related deformation and schematic interpretation. Fig 4A and 4D are representative 2D XRD images for target olivine grains in NWA 2221 (Fig. 4B) and NWA 2737 (Fig. 4E), respectively. They both show mosaic spread along Debye rings indicating the misoriented subdomains due to shock. However, quantitative SRM analysis revealed that NWA 2737 yields higher $\sum(FWHM\chi)$ compared to NWA 2221 (Figure 4C and 4F, resp.), consistent with their shock classifications. Figure 4G is a schematic diagram showing the development of mosaic spread from non-shocked grains to highly shocked grains, with three observed examples shown below (modified after Flemming et al., 2007, Vinet et al., 2010, and Li et al., 2020).

This is the peer-reviewed, final accepted version for American Mineralogist, published by the Mineralogical Society of America.
The published version is subject to change. Cite as Authors (Year) Title. American Mineralogist, in press.
DOI: https://doi.org/10.2138/am-2022-8441. http://www.minsocam.org/

TABLE CAPTION

Table 1 Summary of USL measurements. USL_{robust} used all the boundary lengths regardless of type and $USL_{(tilt + twist)}$ used boundary type estimation to calculate the unit length. Identified tilt boundary and twist boundary occurrences are also listed in the table, identified using the angle leniency as described in Wieser et al., (2020). The sum of tilt and twist boundary length is smaller than the total boundary length, because not all boundaries are identifiable by the angle leniency setup. Overall trend of USL to increase with shock level is consistent between USL_{robust} and $USL_{(tilt + twist)}$.

Table 1 Summary of the USL measurements

		USL_{Robust} (*10^{-2} μm^{-1})	$USL_{Tilt+Twist}$ (*10^{-2} μm^{-1})	Total Boundary Length (*10^{3} μm)	Identified Tilt Boundary* (*10^{3} μm)	Identified Twist Boundary* (*10^{3} μm)	Tilt ratio (Tilt/Total Length)	Measured Grain Area (*10^{5} μm^{2})
Terrestrial Olivine (Wieser et al., 2020)	Target 1	0.36	0.31	11.08	9.01	0.51	0.81	31.03
NWA 2221	Target 1	1.62	1.43	9.65	6.59	1.97	0.68	5.96
	Target 2	3.40	3.19	9.53	7.88	1.04	0.83	2.80
	Target 3	3.40	3.11	23.86	17.35	4.52	0.73	7.02
NWA 2737	Target 1	5.38	4.70	6.26	4.12	1.35	0.65	1.16
	Target 2	4.13	3.51	7.44	5.17	1.14	0.69	1.80
	Target 3	5.26	4.58	6.83	4.46	1.49	0.65	1.30
	Target 4	6.74	5.77	4.73	3.20	0.84	0.68	0.70

*tilt boundary and twist boundary are identified by adopting the method developed by Wieser et al. (2020), which considers the identified boundary as either "pure" tilt or twist. Herein, the some mixtures are excluded if the boundary geometry fails to match with the angle leniency. More detail on this method in text and from Wieser et al.(2020).

Fig 1

Schematic illustration of two types of boundaries

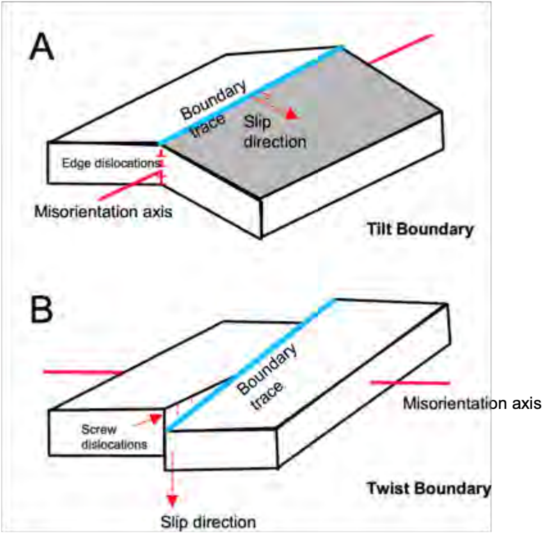

Figure is modified after Wieser et al., (2020)

Fig 2

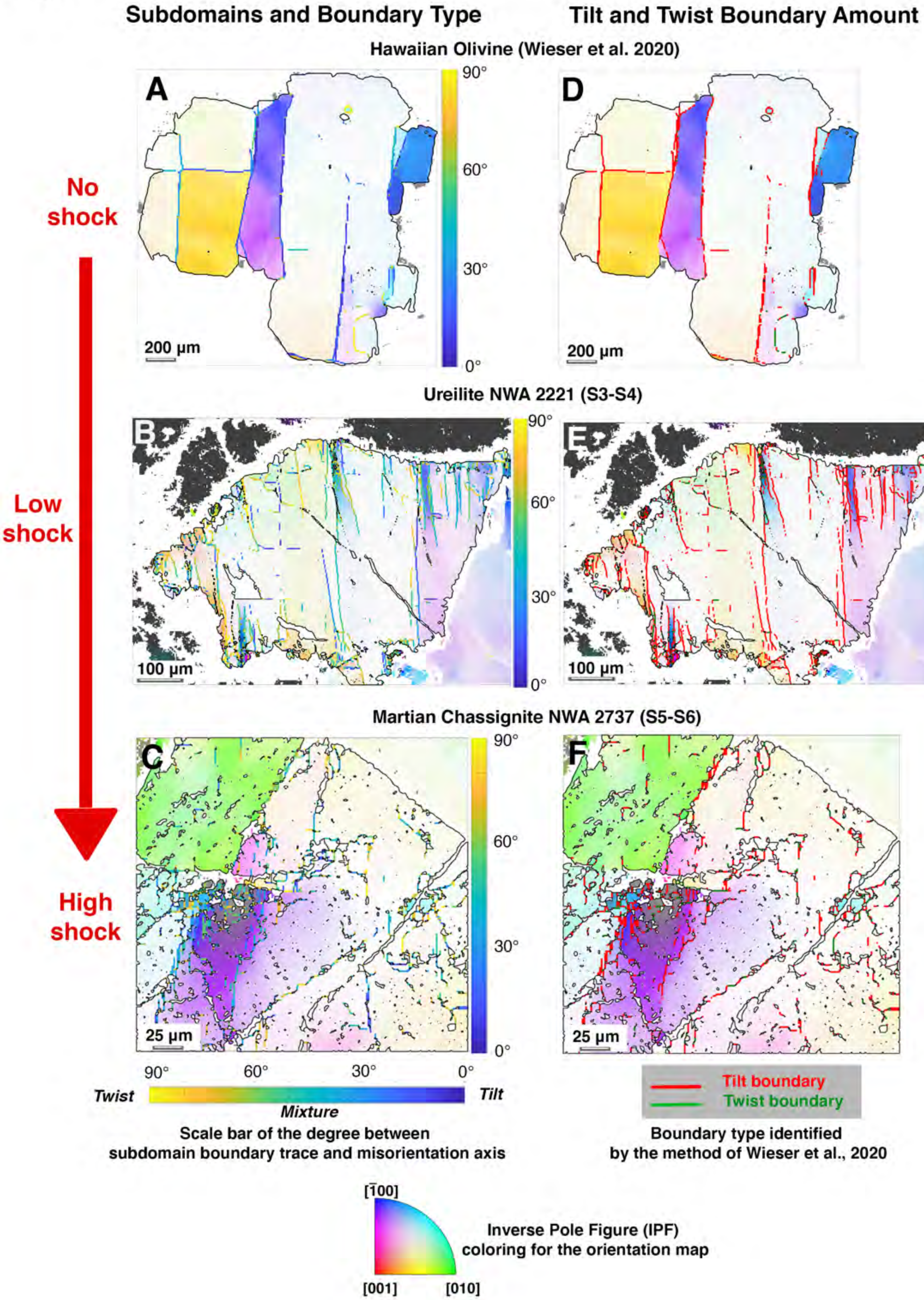

Subdomains and Boundary Type
Tilt and Twist Boundary Amount
Hawaiian Olivine (Wieser et al. 2020)
A
D
90°
60°
30°
0°
200 µm
200 µm
No shock
Low shock
High shock
Ureilite NWA 2221 (S3-S4)
B
E
90°
60°
30°
0°
100 µm
100 µm
Martian Chassignite NWA 2737 (S5-S6)
C
F
90°
60°
30°
0°
25 µm
25 µm
90°
60°
30°
0°
Twist
Tilt
Mixture
Scale bar of the degree between
subdomain boundary trace and misorientation axis
Tilt boundary
Twist boundary
Boundary type identified
by the method of Wieser et al., 2020
[$\bar{1}$00]
[001]
[010]
Inverse Pole Figure (IPF)
coloring for the orientation map

Fig 3

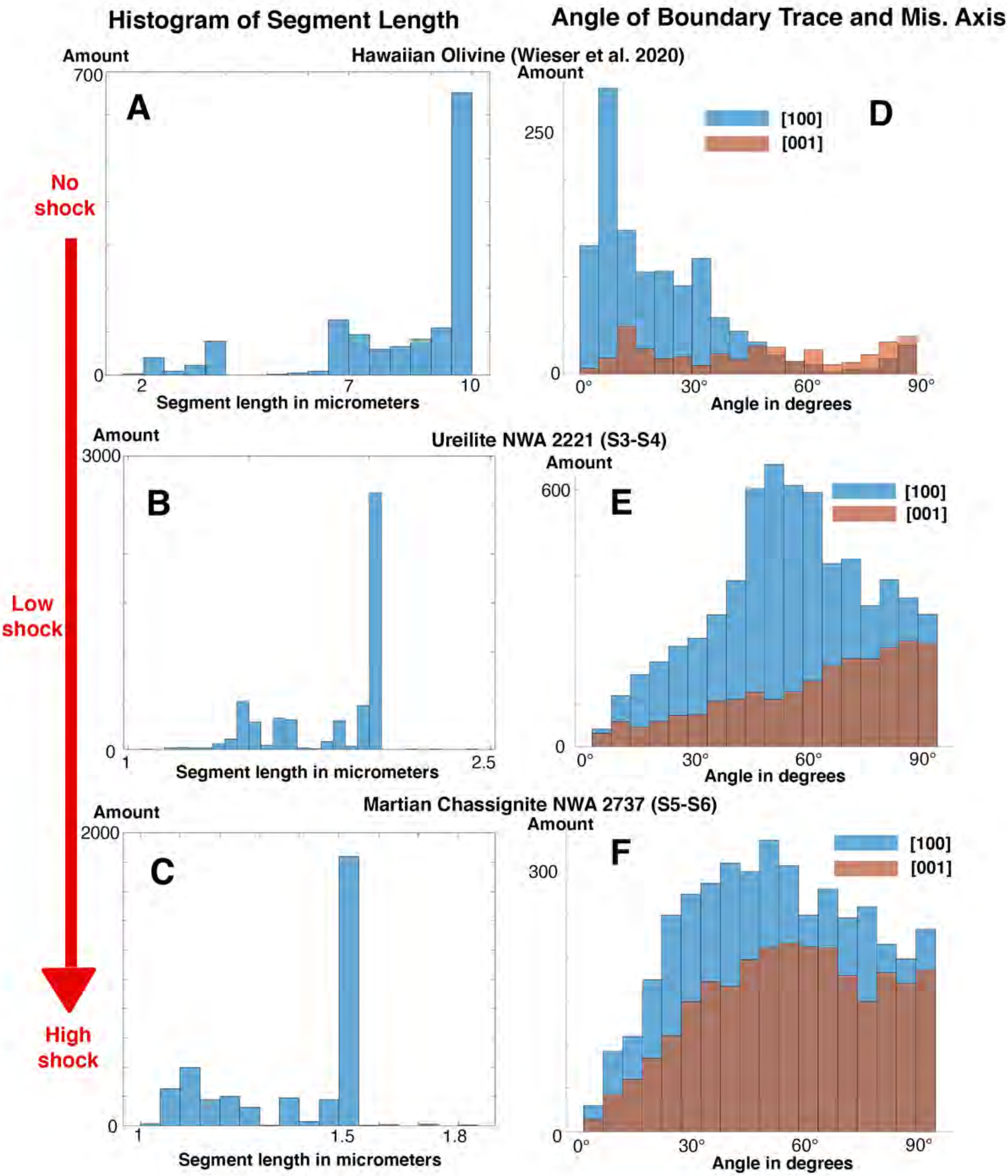
Histogram of Segment Length
Angle of Boundary Trace and Mis. Axis
Hawaiian Olivine (Wieser et al. 2020)
Amount
700
0
A
2
7
10
Segment length in micrometers
Amount
250
0
D
[100]
[001]
0°
30°
60°
90°
Angle in degrees
No shock
Low shock
High shock
Ureilite NWA 2221 (S3-S4)
Amount
3000
0
B
1
2.5
Segment length in micrometers
Amount
600
0
E
[100]
[001]
0°
30°
60°
90°
Angle in degrees
Martian Chassignite NWA 2737 (S5-S6)
Amount
2000
0
C
1
1.5
1.8
Segment length in micrometers
Amount
300
0
F
[100]
[001]
0°
30°
60°
90°
Angle in degrees

Fig 4

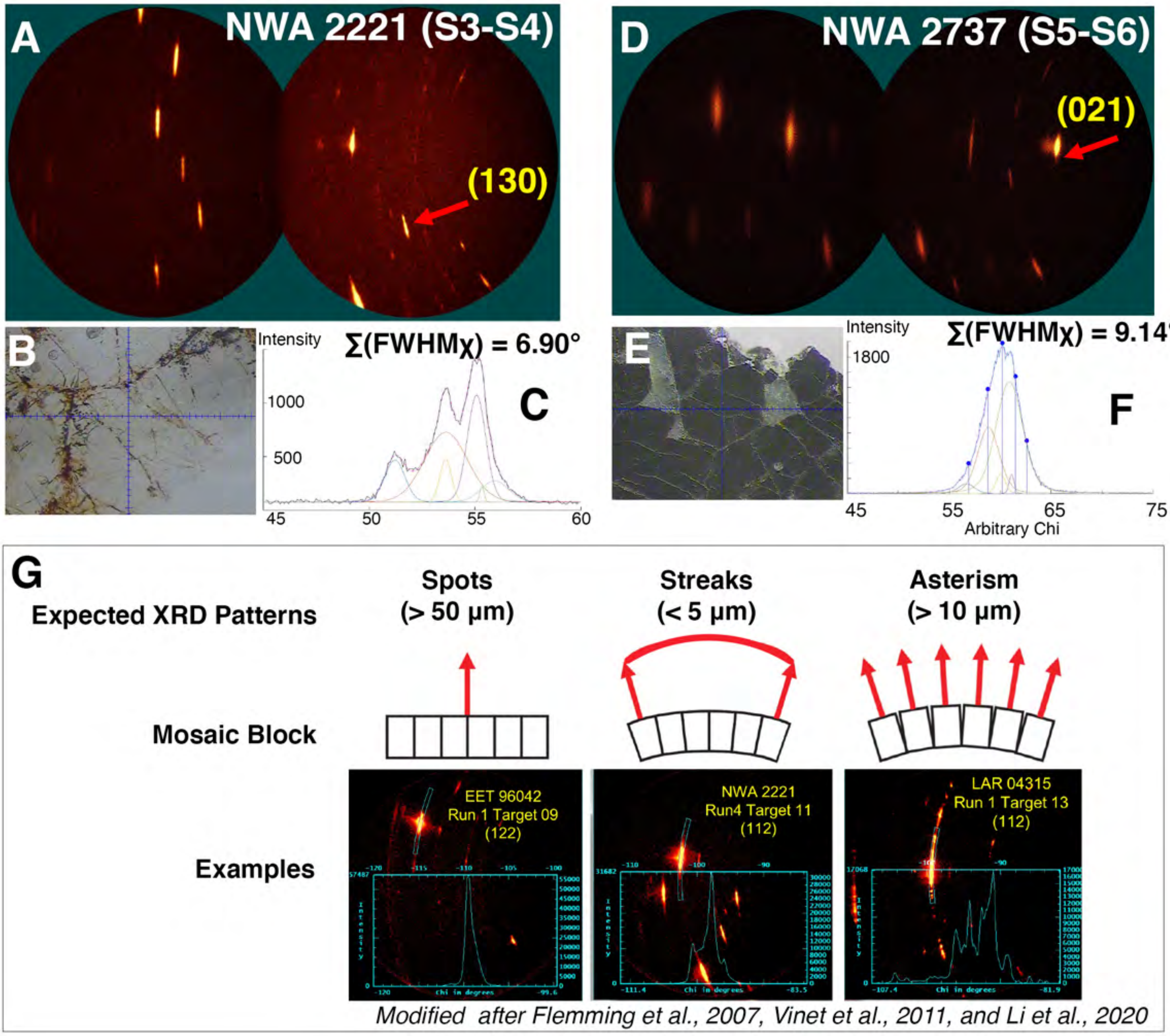

A
NWA 2221 (S3-S4)
(130)
D
NWA 2737 (S5-S6)
(021)
B
Intensity
Σ(FWHMχ) = 6.90°
1000
500
C
45
50
55
60
E
Intensity
Σ(FWHMχ) = 9.14°
1800
F
45
55
65
75
Arbitrary Chi
G
Expected XRD Patterns
Spots
(> 50 μm)
Streaks
(< 5 μm)
Asterism
(> 10 μm)
Mosaic Block
Examples
EET 96042
Run 1 Target 09
(122)
NWA 2221
Run4 Target 11
(112)
LAR 04315
Run 1 Target 13
(112)
Modified after Flemming et al., 2007, Vinet et al., 2011, and Li et al., 2020